Binary bilayer simulations for partitioning within membranes

Soohyung Park^a, Richard W. Pastor^b, and Wonpil Im^a,*

^aDepartments of Biological Sciences and Chemistry, Lehigh University, Bethlehem, PA, United States ^bLaboratory of Computational Biology, National Heart, Lung, Blood Institute, National Institutes of Health, Bethesda, MD, United States

Contents

1.	Arena	124
2.	Binary bilayer system	126
3.	Implementation	127
	3.1 Binary bilayer restraining potential	127
	3.2 Determination of lateral dimensions	129
	3.3 Generation of binary bilayer system	130
4.	Preliminary symmetric bilayer simulations	132
5.	Equilibration of individual bilayers	134
6.	Assembly of the binary bilayer system	134
	6.1 Preparation for equilibration and production simulations	136
	6.2 Verification of lateral packing in BBS	138
	6.3 Examples	140
	6.4 Parameter tuning	145
	6.5 What can go wrong?	146
7.	Performance	147
	7.1 Advantages	147
	7.2 Limitations	148
8.	Alternatives	148
9.	Outlook	150
10.	Connections	151
Acknowledgements		152
References		152

Abstract

Membrane proteins (MPs) often show preference for one phase over the other, which is characterized by the partition coefficient, K_p . The physical mechanisms underlying K_p have been only inferred indirectly from experiments due to the unavailability of detailed structures and compositions of ordered phases. Molecular dynamics (MD) simulations can complement these details and thus, in principle, provide further insights into the partitioning of MPs between two phases. However, the application of

^{*}Corresponding author. e-mail address: wonpil@lehigh.edu

MD has remained difficult due to long time scales required for equilibration and large system size for the phase stability, which have not been fully resolved even in free energy simulations. This chapter describes the recently developed binary bilayer simulation method, where the membrane is composed of two laterally attached membrane patches. The binary bilayer system (BBS) is designed to preserve the lateral packing of both phases in a significantly smaller size compared to that required for macroscopic phase separation. These characteristics are advantageous in partitioning simulations, as the length scale for diffusion across the system can be significantly smaller. Hence the BBS can be efficiently employed in both conventional MD and free energy simulations, though sampling in ordered phases remains difficult due to slow diffusion. Development of efficient lipid swapping methods and its combination with the BBS would be a useful approach for partitioning in coexisting phases.

1. Arena

Phase separation is observed in both synthetic and biological membranes, and in monolayers. Examples include liquid ordered (Lo) and liquid disordered (Ld) domains in multi-component bilayers (Feigenson, 2009; Veatch & Keller, 2003), cholesterol-driven and phosphatidylinositol 4,5-bisphosphate (PIP₂)-driven rafts in cell membranes (Pike, 2006; Sezgin, Levental, Mayor, & Eggeling, 2017), and liquid condensed (Lc) and liquid expanded (Le) phases in model and pulmonary monolayers (Casals & Cañadas, 2012; Parra & Pérez-Gil, 2015; Wüstneck et al., 2005). Membrane proteins (MPs) often show preference to one phase over the other due to different interactions with these phases arising from differences in lateral packing and compositions. The preference is characterized by the partition coefficient, K_p , which is calculated as the ratio of concentrations (typically determined through fluorescence intensities) of MPs in ordered and disordered phases (Levental, Lingwood, Grzybek, Coskun, & Simons, 2010).

It has been observed that in cell-derived giant plasma membrane vesicles (GPMVs) K_p of MPs increases with the lipidation and the length of the transmembrane domain (Diaz-Rohrer, Levental, Simons, & Levental, 2014; Levental et al., 2010; Van Duyl, Rijkers, Kruijff, & Killian, 2002; Zhang, Trible, & Samelson, 1998), and decreases with a larger accessible surface area (Lorent et al., 2017). However, in synthetic giant unilamellar vesicles (GUVs) composed of a few lipid types, MPs prefer disordered phases, including those that favor the ordered phase in GPMVs (Bacia, Schuette, Kahya, Jahn, & Schwille, 2004; Kahya, Brown, & Schwille, 2005; Shogomori et al., 2005). The physical mechanisms underlying such different observations between GPMVs and GUVs can be only inferred indirectly because detailed structures and compositions of ordered phases in the former are unknown.

Molecular dynamics (MD) simulations can complement these experiments and thus, in principle, can provide further insights into the partitioning of MPs between ordered and disordered phases. However, the application of conventional MD to partitioning in membranes has remained difficult. One obvious problem is the long time scale required for equilibration in the ordered phase due to slow diffusion. For example, the saturated chain contacts in the Lo phase core have lifetimes of ~400 ns in the Lo phase of ternary mixed bilayer composed of a total of a few hundred dioleyoylphosphatidylcholine (DOPC), dipalmitoylphosphatidylcholine (DPPC), and cholesterol (Chol) (Sodt, Sandar, Gawrisch, Pastor, & Lyman, 2014), implying that the equilibration requires multi-us time scales. Another difficulty is the system-size dependent stability of phases. For macroscopic phase separation (where properties are not system-size dependent), the system size should be larger than its critical size (~1500 lipids for a coarse-grained (CG) ternary mixed bilayer composed of DPPC, dilinoleoylphosphatidylcholine (DIPC), and Chol) (Pantelopulos, Nagai, Bandara, Panahi, & Straub, 2017), otherwise only nanoscale ordered phases can exist in the membrane. Hence, large system size and long trajectories are required to calculate partitioning between macroscopically separated phases using conventional MD. Currently, the required length and time scales are not accessible without using specially designed computers for MD, such as Anton (Shaw et al., 2014).

The time scale and phase stability issues can be avoided or overcome (at least partly) in free energy simulations along either physical or alchemical reaction coordinates. One available approach is the indirect insertion free energy method (Bereau, Bennett, Pfaendtner, Deserno, & Karttunen, 2015; Lopez, de Vries, & Marrink, 2013; Zhang, Lu, & Berkowitz, 2008), which is conceptually analogous to Chol exchange experiments between β -cyclodextrin (β -CD) and different vesicles (Leventis & Silvius, 2001; Niu, Mitchell, & Litman, 2002; Ohvo-Rekilä, Åkerlund, & Slotte, 2000). More recently, the umbrella sampling (US) method has been employed to directly calculate the free energy profile across ordered and disordered phases (Lin, Gorfe, & Levental, 2018; Lorent et al., 2017). Another available approach is an alchemical free energy method developed to compare the free energy difference between two structurally similar MPs in a membrane (Gumbart & Roux, 2012). An alchemical method has also been applied to understand the driving force for the formation of coexisting Lo-Ld phases by calculating the exchange free energy of saturated and unsaturated lipids in Lo and Ld phases (Bennett, Shea, & Tieleman, 2018).

While insertion and alchemical free energy approaches for partitioning between membrane phases (or compositions) can be useful, they are computationally intensive due to the requirement of a reference medium and a large number of windows along reaction coordinates. Direct US for macroscopically separated Lo and Ld phases would be computationally even more intensive due to the required large system size. Thus, it is of interest to have a more practical simulation method for partitioning between moderate-sized membranes with well-maintained interfaces without the need of a reference medium. To this end, we developed the binary bilayer simulation method for partitioning between membrane phases or compositions (Park & Im, 2018).

2. Binary bilayer system

A binary bilayer system (BBS) is composed of two laterally attached membrane patches, B1 and B2 (red and blue in the schematic shown in Fig. 1). In the present work, these patches are arranged along the lateral dimension X (length L_X). The mixing between bilayers is prevented by applying a soft restraining potential to each of specified lipids assigned to each bilayer. The restraining potential applied to a lipid starts acting when it diffuses beyond a pre-defined margin (X_M) along the X-dimension into its counterpart membrane (blue and red arrows). The margin X_M gives room to self-adjust the lateral packing of each patch and thereby maintain the corresponding single membrane. We denote the restraining potential as the BBS restraining potential, V(X). The unrestrained components in the BBS can freely diffuse across interfaces. An ideal BBS is defined when the two patches are surface area (SA) matched and their boundaries are aligned to the Y-axis (located at X = 0 and at $X = \pm L_X/2$ in CHARMM convention).

The simulation of a BBS can be run without any hard-code implementation in all major MD packages that support imposing an external global potential V(X) such as CHARMM (Brooks et al., 2009), NAMD (Phillips et al., 2020), GROMACS (Abraham et al., 2015), and OpenMM (Eastman et al., 2017). To prepare a BBS and to apply V(X) to individual lipids, basic knowledge in each MD engine and script languages (such as shell and python) are required. Therefore the BBS can be a practically useful platform for partitioning membrane simulations, as compositions of each leaflet in two membrane patches can be arbitrary because the membrane-membrane interfaces are prevented from dissolving by V(X). A conventional MD or an US free energy simulation along the X-dimension can be chosen for a BBS, depending on the lateral packing in the two patches. Conventional MD can be efficient for partitioning between these patches for fast diffusing molecules, as was done to examine Chol preference between different lipids (Park & Im, 2018). US MD can be applied

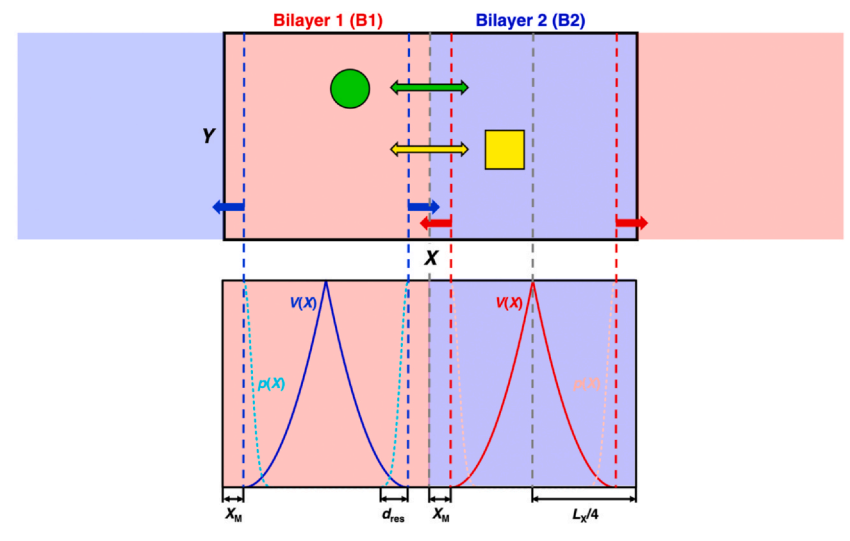


Fig. 1 (Top) Schematic of a binary bilayer system (BBS), where two membrane patches are laterally attached (enclosed by a black rectangle). Their interfaces are maintained by soft restraining potentials (blue and red arrows) applied to specific lipids when they cross the pre-defined X-positions (red and blue dotted vertical lines) in the center and edges of the periodic cell. The unrestrained components can freely diffuse across interfaces (green and yellow). Adapted with permission from Reference Park, S., & Im, W. (2018). Quantitative characterization of cholesterol partitioning between binary bilayers. *Journal of Chemical Theory and Computation*, *14*(6), 2829–2833, https://doi.org/10.1021/acs.jctc.8b00140. Copyright 2018 American Chemical Society. (Bottom) The binary bilayer restraining potential, V(X) (Eq. (1)), and the corresponding lipid distribution, p(X) (Eq. (2)), in the counterpart bilayers. V(X) for lipids belonging to bilayers 1 and 2 are shown in red and blue solid lines, respectively. The corresponding lipid distribution, p(X) are shown in pink and cyan dotted lines, respectively. $X_{\rm M}$ is a distance from the bilayer-bilayer interface that V(X) starts acting, and $d_{\rm res}$ is the penetration depth from $X_{\rm M}$ (Eq. (3b)).

when diffusion of the partitioning molecule is slow (Park, Yeom, Andersen, Pastor, & Im, 2019), and when liquid ordered phases are involved (Park, Levental, Pastor, & Im, 2023).



3. Implementation

3.1 Binary bilayer restraining potential

The simplest choice for the restraining potential is an inverted flat-bottomed harmonic potential. For a lipid i, the restraining potential is defined as

$$V(X_{i}) = \begin{cases} \frac{k_{r}}{2} (|X_{i} - X_{\text{ref},i}| - w_{r})^{2}, & \text{if } |X_{i} - X_{\text{ref},i}| < w_{r} \\ 0, & \text{otherwise} \end{cases}$$
(1)

where X_i is the X-position of the lipid i, k_r is the force constant, and $X_{\text{ref},i}$ is the X-center of the counterpart membrane of the lipid i, which is $X_{\text{ref},i} = L_X/4$ when the lipid is initially at X < 0 and vice versa. Here, $w_r = L_X/4 - X_M$ is the half-width of the X-range of the non-vanishing restraining potential (V(X) > 0, see Fig. 1).

The effects of V(X) on the BBS can be analyzed by considering the distribution of restrained lipids. Assuming that the potential energy distribution of lipids obeys the Boltzmann distribution and the lipid penetration into the counterpart membrane does not extend to its X-center, the distribution of restrained lipids can be described using a half-sided Gaussian (Fig. 1). Let us consider a type of restrained lipids whose initial positions were at X < 0. In an ideal BBS (with the membrane-membrane interfaces parallel to the Y-axis), the first half of their distribution in a X-range, $[X_M, L_X/4]$, is accurately approximated as a half-sided Gaussian distribution, p(X), defined for $X \ge X_M$,

$$p(X) = \frac{2}{\sqrt{2\pi}\sigma} \exp\left[-\frac{(X - X_{\rm M})^2}{2\sigma^2}\right]$$
 (2)

where $\sigma = (k_{\rm B}T/k_{\rm r})^{1/2}$. The other half of the distribution in a X-range, $[L_{\rm X}/4, L_{\rm X}/2-X_{\rm M}]$ is similarly approximated as the mirror image of Eq. (2) with respect to the axis of symmetry at $X = L_{\rm X}/4$. Thus the fraction of restrained lipids, $f_{\rm res}$, can be obtained from the integral of Eq. (2).

$$f_{\text{res}} = 2 \frac{c(X_{\text{M}})}{N_0} \frac{\sqrt{2\pi}\sigma}{2} \int_{X_{\text{M}}}^{\infty} dX \quad p(X) \stackrel{X_{\text{M}}=0}{\to} \sqrt{2\pi} \frac{d_{\text{res}}}{L_X}$$
(3a)

where the factor 2 in the middle term in Eq. (3a) takes into account lipidpenetrations across two interfaces (at X = 0 and $X = L_X/2$), $c(X_M)$ is the number density of lipids along the X-dimension at $X = X_M$, and N_0 is the total number of the lipids. Here, d_{res} is the root-mean square penetration depth, obtained from the second moment of p(X)

$$d_{\text{res}} = \left[\int_{X_{\text{M}}}^{\infty} dX (X - X_{\text{M}})^{2} p(X) \right]^{1/2} = \sigma = \sqrt{\frac{k_{\text{B}} T}{k_{\text{r}}}}$$
(3b)

which is inversely proportional to the square root of k_r . The fraction of highly restrained lipids (whose $V(X) > 2k_BT$), f_{hres} , is obtained as

$$f_{\text{hres}} = \sqrt{2\pi} d_{\text{res}} \frac{c(X_{\text{M}})}{N_0} \int_{X_{\text{M}} + 2\sigma}^{\infty} dX \quad p(X) = f_{\text{res}} \operatorname{erfc}(\sqrt{2})$$
(3c)

where $\operatorname{erfc}(X) \equiv 1 - \operatorname{erf}(X)$ is the complementary error function. We note that the fractions of restrained lipids, f_{res} and f_{hres} , are inversely proportional to $L_X k_r^{1/2}$. The total restraining energy, E_{res} , can be also obtained from the second moment as

$$E_{\text{res}} = \sqrt{2\pi} \, d_{\text{res}} \, \epsilon \left(X_{\text{M}} \right) \int_{X_{\text{M}}}^{\infty} dX \quad V\left(X \right) p\left(X \right) = \frac{k_{\text{B}} T}{2} N_0 f_{\text{res}}$$
(3d)

which is equivalent to the mean thermal energy partitioned to the X-dimension ($k_{\rm B}T/2$) multiplied by the number of restrained lipids ($N_0f_{\rm res}$).

Immediate implications from Eq. (3) are: (1) effects of V(X) to the membrane properties becomes less significant with increasing L_X ; (2) the sharpness and ruggedness of the bilayer-bilayer interfaces can be controlled by tuning k_r and X_M , and the inner region of each patch farther than a X-distance, $d_{\text{res}} + X_M$, from the membrane-membrane interfaces are not influenced by V(X); (3) E_{res} can be tuned by adjusting the aspect ratio, $L_X:L_Y$ ($N_0 \propto L_XL_Y$).

3.2 Determination of lateral dimensions

Before generating a BBS, one needs to determine reasonable lateral dimensions, L_X and L_Y , for which we assume that component APLs for a chosen lipid composition do not vary with the system size. We also assume that inclusion of a MP does not perturb component APLs. With these assumptions, we provide criteria for the minimum lateral dimensions of a BBS.

For a BBS with an embedded MP, the box size of each bilayer along the X-dimension ($L_X/2$) can be chosen from the following criterion.

$$L_X/2 \ge L_{\min,X} = 2(l_P + 3l_L + d_{res} + X_M)$$
 (4a)

where $l_{\rm P} = A_{\rm P}^{-1/2}$ is the effective lateral dimension of the MP with an area of $A_{\rm P}$, and $l_{\rm L} = A_{\rm L}^{-1/2}$ is the mean lateral dimension of a lipid with a mean area of $A_{\rm L}$ (typically $\sim 60\text{--}70\,\text{Å}^2$). Here, $L_{\rm min,X}$ is the minimum box size along the X-dimension, which can include at least three lipid shells around the MP in the inner region of a bilayer. This criterion is based on the bilayer deformation around gramicidin A (gA), which is relaxed over the first three

lipid shells (Kim et al., 2012). From the same criterion, one can easily find that $L_Y \ge L_{\min,X}$ and an aspect ratio, $L_X:L_Y = 2:1$ for a BBS with an embedded MP is a natural choice.

Another criterion is obtained from a consideration of A_P , SA difference between two individual bilayers, Δ SA, and the area of the mixing zone of a bilayer, $2X_ML_Y$. Let us consider a case that a MP at the XY center of B1 partitioned to B2. After the MP's partitioning, the SA of B1 is decreased by A_P . This area change in the core region should be compensated by lipids in the mixing zone to preserve its lateral packing, that is, the area of the mixing zone should be larger than A_P . At the same time, the mixing zone should be able to buffer Δ SA. Thus, we obtain the second criterion,

$$L_Y \ge L_{\min,Y} = \frac{A_P + \Delta SA}{2X_M} \tag{4b}$$

While the criterion given by Eq. (4b) is typically satisfied for a small MP, it still provides a useful guideline for the width of the mixing zone, that is, $X_{\rm M}$.

From these criteria, the lateral dimensions of a BBS, L_X and L_Y , can be chosen arbitrarily providing that

$$L_X \ge 2L_{\min,X}$$
 (5a)

$$L_Y \ge \max\{L_{\min,X}, L_{\min,Y}\}$$
 (5b)

For a small MP (e.g., a single pass transmembrane helix) whose $l_{\rm P} \sim 10$ Å, $L_{{\rm min},X} \sim 86$ Å and $L_{{\rm min},Y} \sim 25$ Å from Eq. (4) when $d_{\rm res} \sim 1$ Å, $l_{\rm L} \sim 8$ Å, $X_{\rm M} \sim 4$ Å, and $\Delta {\rm SA} \sim 100$ Å². An estimate of the number of lipids (APL ~ 64 Å²) in a leaflet of the corresponding patch (SA of $L_{{\rm min},X}^2$) is around 116. Although a larger system size can be chosen, we recommend a comparable system size to the estimate from Eq. (5) for computational efficiency. The determined L_X and L_Y are used to estimate the number of lipids in each leaflet in each bilayer in the BBS.

3.3 Generation of binary bilayer system

For the chosen lateral dimensions of a BBS $(L_X \times L_Y)$, one of the simplest and most straightforward approaches for its generation is splicing two SA-matched bilayer patches (SA of $L_X/2 \times L_Y$). Its generation workflow consists of three steps (Fig. 2): (1) Preliminary symmetric bilayer simulations; (2) Equilibration of individual bilayers; (3) Assembly of the BBS. These steps are described in detail below with an example of the generation of a BBS composed of Lo and Ld phase bilayers, which are composed of

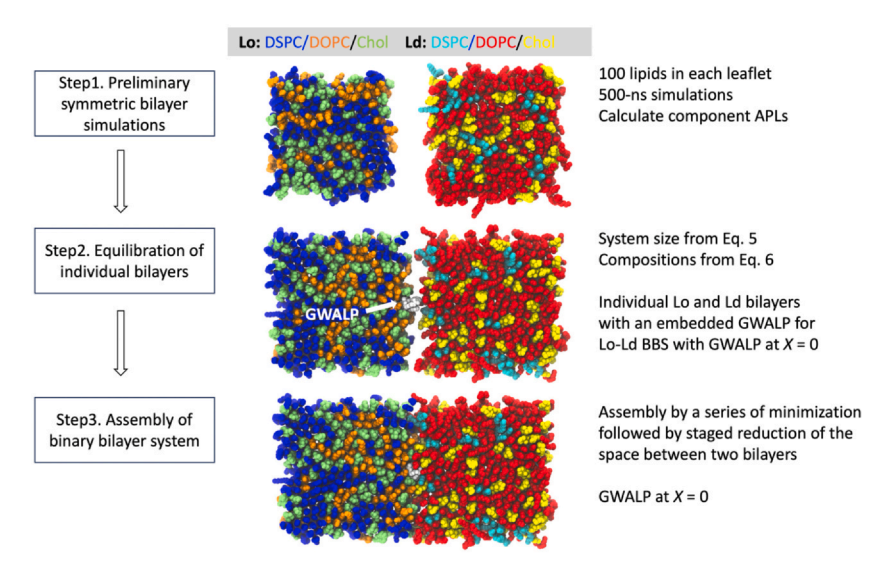


Fig. 2 Workflow of binary bilayer system generation. In snapshots, only heavy atoms of cholesterol, lipid tail, and a model transmembrane peptide, GWALP, are shown for clarity. Color code is given in the figure.

distearoylphosphatidylcholine (DSPC), DOPC, and Chol. The Lo and Ld compositions are chosen to be close to those in the high tie-line of the ternary phase diagram (Konyakhina, Wu, Mastroianni, Heberle, & Feigenson, 2013; Usery et al., 2018). In the BBS, a small model transmembrane helix (TM), GWALP, is embedded at the interface between Lo and Ld phases (X=0), whose sequence is acetyl-GGAFF(LA)₆LWLAGA-amide.

In the example, individual bilayers for steps 1 and 2 were prepared using CHARMM-GUI *Membrane Builder* (Jo, Kim, & Im, 2007; Jo, Kim, Iyer, & Im, 2008; Jo, Lim, Klauda, & Im, 2009; Lee et al., 2019; Wu et al., 2014). One GWALP was embedded in the Lo phase bilayer in step 2 for the assembly of BBS with the embedded GWALP. All bilayer simulations were carried out using OpenMM with CHARMM36(m) protein (Huang & Mackerell, 2013) and lipid (Klauda et al., 2010) force fields and TIP3P water model (Durell, Brooks, & Bennaim, 1994; Jorgensen, Chandrasekhar, Madura, Impey, & Klein, 1983; Neria, Fischer, & Karplus, 1996). The van der Waals interactions were smoothly switched off over 10–12 Å by a force-based switching function (Steinbach & Brooks, 1994), and the electrostatic interactions were calculated using the particle-mesh Ewald method (Essmann et al., 1995). Covalent bonds involving hydrogen atoms were constrained using the SHAKE algorithm

(Ryckaert, Ciccotti, & Berendsen, 1977). Temperature and pressure were set to $T = 298.15 \,\mathrm{K}$ and $p = 1 \,\mathrm{bar}$, which were controlled by Langevin dynamics with a friction coefficient of $1 \,\mathrm{ps}^{-1}$ and a semi-isotropic Monte Carlo barostat with a pressure coupling frequency of 100 steps, respectively (Åqvist, Wennerström, Nervall, Bjelic, & Brandsdal, 2004; Chow & Ferguson, 1995). The semi-isotropic barostat (typically applied to membrane simulations) allows isotropic fluctuations in the lateral (XY) dimensions with an independent fluctuation along the Z-dimension. While one may consider other type of barostat, for example, anisotropic pressure coupling to Y and Z dimensions with fixed X-dimension, we recommend using the semi-isotropic barostat because it better mimics the volume fluctuations of individual membranes and allows even SA changes along the lateral dimensions.

Bilayers were equilibrated following the six-step protocol employed in *Membrane Builder* (Jo et al., 2007), which consists of a series short constant volume and temperature (NVT) and constant pressure and temperature (NPT) simulations with integration time steps of 1–2 fs. Various restraints applied to hold the positions and dihedral angles of lipid (and GWALP) were gradually relaxed to vanish during the equilibration. For steps 1 and 2, 500-ns and 4-µs production simulations were carried out, respectively, with an integration time step of 4 fs with the hydrogen mass repartitioning technique (Gao et al., 2021; Hopkins, Le Grand, Walker, & Roitberg, 2015). The finial snapshots of individual bilayers from step 2 were used to assemble the BBS in step 3. The lipid compositions for Lo and Ld phase bilayers for steps 1 and 2, and component APLs from step 1 are listed in Table 1.

4. Preliminary symmetric bilayer simulations

In this preliminary equilibration step, for unique lipid compositions of leaflets in two bilayers, corresponding symmetric bilayers (without a MP) are prepared, whose system sizes are comparable to or smaller than the target SA, $L_XL_Y/2$. These symmetric bilayers and associated inputs for various MD engines can be conveniently generated using *Membrane Builder*. Generated symmetric bilayers are simulated under the same conditions for the BBS (e.g., at the same pressure, p, and temperature, T, for NPT simulations). For each symmetric bilayer, the simulation is carried out until its system size (i.e., the lateral packing) stabilizes (typically a few hundred ns). From the equilibrated trajectories, the component area per lipid (APL) can be calculated by a Voronoi tessellation approach using either available analysis codes

t (µs) 0.5 0.5 0.4 6.0 27.5 (0.3) 29.8 (0.5) Chol Component APL (Å2) 51.0 (1.4) 58.1 (0.7) DOPC 49.5 (0.3) 56.3 (0.8) DSPC Table 1 System information of Lo and Ld bilayers for steps 1 and 2. Chol 40 31 54 35 Number of lipids DOPC 20 28 99 27 DSPC 40 1 12 54 $Lo+GWALP^a$ Ld (sm.) Lo (sm.) System^a Γd^a

"GWALP is a 23 residue model transmembrane peptide, whose sequence is acetyl-GGAFF(LA)6LWLAGA-amide. Lo (sm.) and Ld (sm.) are smaller symmetric Lo- and Ld-phase bilayers, from which component area per lipids were calculated. The number of each lipid types for Lo+GWALP and Ld are calculated using Eqs. (5) and (6). (e.g., MEMBPLUGIN module (Guixà-González et al., 2014) in VMD (Humphrey, Dalke, & Schulten, 1996) and APL@Voro (Lukat, Krüger, & Sommer, 2013)) or in house scripts (Pandit et al., 2004). The calculated component APLs from each symmetric bilayers are used to estimate the number of lipids for each lipid type in the corresponding leaflet in the BBS. For a bilayer Bi in the BBS, the numbers of lipids are calculated from

$$\sum_{j} N_{j,B_i} A_{j,B_i} = L_X L_Y / 2 \tag{6}$$

where j is the lipid component index, $N_{j,Bi}$ is its number, and $A_{j,Bi}$ is its APL. The determined number of lipids for each leaflet will be used to generate individual bilayers in the BBS.

5. Equilibration of individual bilayers

For the determined number of lipids for each leaflet, individual bilayers and associated inputs for simulations can be easily prepared using Membrane Builder. The equilibration can be simply a few hundred ns for SA equilibrated bilayers (as described above). For well-equilibrated structures in ordered phases, a longer simulation time (multi-µs) is required. For a moderate-sized BBS (composed of a few hundred lipids), it is feasible to equilibrate individual bilayers up to a few µs using computers with graphics processing units (GPUs). A MP is embedded in one of the two bilayers depending on its X-position in the BBS. When the embedded MP would be located near the bilayer-bilayer interfaces (interacting with both bilayers) in the assembled BBS, the MP is embedded in the ordered phase bilayer for the equilibration, which is subject to pulling to the target position after the assembly. The final snapshots of equilibrated bilayers are then prepared for the assembly of the BBS, where the Y center of mass (Y_{COM}) of the embedded MP is aligned to the Y center of the bilayer (Y = 0 in CHARMM convention) and the X center of mass (X_{COM}) of the MP is aligned accordingly to its X-position in the BBS (within the box edge of the bilayer) to prevent clashes between the MP and the other bilayer.

6. Assembly of the binary bilayer system

In this step, two individual bilayers from the previous step are assembled to a BBS. Here, we explain the assembly using CHARMM (all input files are

available at https://github.com/spark-94/BBS.git). The bilayers are first arranged in a BBS with a larger X-dimension so that there is no contact between bilayers. More specifically, the target L_X of the bilayer is $L_X = 2 \max\{L_{X,B1}, L_{X,B2}\}$, where $L_{X,Bi}$ is the X-dimension of the bilayer Bi (i = 1 or 2). The bilayers, B1 and B2, are arranged so that their interface is located at X = 0 by translating along the X-dimension by $(-1)^i L_{X,Bi}/2$ (i = 1 or 2). Then, the bilayer Bi is additionally translated by $dL_{XI,Bi} = (-1)^i [(X_{\max,Bi} - X_{\min,Bi}) - L_{X,Bi}]/2$, to allow a small space between B1 and B2 along the X-dimension. Here, $X_{\min,Bi}$ and $X_{\max,Bi}$ are the minimum and maximum X-positions of heavy atoms in the bilayer Bi. The initial box size along the X-dimension, L_{XI} , is set to $L_{XI} = L_X + 2(dL_{XI,B2} - dL_{XI,B1})$ so that the bilayers do not touch each other or their images along the X-dimension. When the embedded MP has large extra-and/or intra-cellular domains, overlapping water molecules are deleted.

A series of minimizations and staged reductions of X-dimension of the BBS follows. In each minimization step, the position restraints are applied to the MP and dihedral restraints are applied to preserve conformations of double bonds (cis and trans), glycerol backbones, and other chiral lipid components such as saccharides using a slightly modified script provided by *Membrane Builder* (see Table 2 for modifications).

Followed by the minimization, the X-dimension of the BBS is reduced by $(L_{X,icycl} - L_X)/2$, where icycl is the minimization cycle number $(L_{X,1} = L_{XI})$. At the same time, to adapt the reduced box size, the bilayer Bi is translated by $-dL_{X,Bi}/2^{icycl}$ toward X = 0. The minimization step is iterated until the system size reaches its target value within 1 Å $(L_{X,icycl} - L_X < 1$ Å) (Fig. 2) (six iterations for our example). This minimization cycle is analogous to that in a conversion algorithm of a bilayer under P2₁ to P1 periodic boundary conditions (Dolan, Venable, Pastor, & Brooks, 2002). In addition, when two bilayer's Z-dimensions, $L_{Z,B1}$ and $L_{Z,B2}$, are significantly different, water and ions from thicker bulk regions can be translated to reduce their difference for smoother equilibration of the assembled BBS. Analogous assembly steps can be performed using other MD packages as well.

For US simulations, this assembly step is repeated for each window from snapshots of individual bilayers whose MP is aligned accordingly to the target X-position in the BBS. When the embedded MP in the assembled BBS is interacting with both bilayers, additional pulling toward the disordered phase bilayer can be performed to match its $X_{\rm COM}$ with the target X-position (as the MP is embedded in the ordered phase in step 2).

Table 2 Modifications in setup_dihe_rest.str from membrane_restraint2.str.

```
>! Parameter from main script
>! TMP : selection for lipids (one atom for each lipid)
>
calc NLipid = ?nsel
23,24c26
< define target sele segid MEMB .and. resid @i end
coor stat sele target end
---
define XX sele TMP .subset. @i end
27a30

define target sele segid @{segid} .and. resn @{lipid} .and. resid @{resid} end
```

6.1 Preparation for equilibration and production simulations

The assembled BBS is subject to further equilibration before production runs, during which the box sizes of two bilayers are adapted to those of the BBS. For these simulations, the restraining potential, V(X) (Eq. (1)), needs to be specified (and updated appropriately). V(X) can be applied either to specific atoms or the center of mass $X_{\rm COM}$ of each component to be restrained. For an NVT simulation, V(X) can be set at the start of simulation for the whole simulation time. For an NPT simulation, box-size related parameters in V(X) ($X_{\rm M}$, $X_{\rm REF,i}$) are updated regularly (e.g., every 1 ns) to reflect the box size change during the simulation. This update can be easily done because V(X) can be set up at the start of each continuation run from the previous simulation (of the same time length to the update interval). For US simulations, the umbrella potential, U(X), for the MP needs to be applied as well.

To specify restraints, index lists for V(X) and U(X) are required. These can be generated at the start of each simulation or saved in separate files for the later use. Both potentials can be conveniently set up easily in most available MD packages using internally supported restraints or external plugins: MMFP module (Brooks et al., 2009) in CHARMM, Colvar module (Fiorin, Klein, & Hénin, 2013) in NAMD, harmonic restraints or PLUMED plugin (Bonomi et al., 2009; The PLUMED consortium, 2019; Tribello, Bonomi, Branduardi, Camilloni, & Bussi, 2014) in GROMACS, to name a few.

While the aspect ratio, $L_X:L_Y$, of the assembled rectangular-shaped BBS is fixed in NVT and NPAT (constant pressure, surface area, and temperature) simulations, it can vary significantly from its initial value in NPT simulations with anisotropic pressure coupling. Semi-isotropic pressure coupling has been

< : from membrane_restraint2.str; > : from setup_dihe_restr.str.

used for membranes with a constant $L_X:L_Y$, which is supported in most MD packages including CHARMM, OpenMM, NAMD, GROMACS. However, the constant aspect ratio in CHARMM is allowed only for tetragonal systems ($L_X:L_Y=1:1$) in NPT simulations (this was employed for Chol partitioning (Park & Im, 2018)). Hence, other MD packages are required for BBS NPT simulations with other aspect ratios (including $L_X:L_Y=2:1$ employed in our example). Below, we show examples for OpenMM equilibration and NPT simulations (all input files are available at https://github.com/spark-94/BBS.git). For other MD packages, inputs can be prepared by an analogous manner.

Generation of system information and translation of initial coordinates.

- Following the format of the crystal constants, {"dimensions": $[L_X, L_Y, L_Z, 90.0, 90.0, 90.0]$ }, provided by *Membrane Builder* (sysinfo.dat), the system information is prepared accordingly, where the lengths $(L_X, L_Y, \text{ and } L_Z)$ are in the units of Å.
- The initial coordinates (in PDB and CRD formats) for OpenMM are prepared from those generated by CHARMM by a translation of a half-box size along all X-, Y-, and Z-dimensions so that its box center is located at $(L_X/2, L_Y/2, L_Z/2)$.
- Lists of atom indices for V(X) (lipid_pos.txt) and U(X) (prot_pos.txt) are prepared by subtracting 1 from the corresponding atom indices in CHARMM because the atom index starts from 0 to 1 in OpenMM and CHARMM, respectively. We do not generate lists for dihedral restraints because the starting configuration was prepared from equilibrated individual bilayers. The formats of these atom index lists are provided in Table 3.

Table 3 File format of atom index lists for OpenMM simulation.FilenameFormat

1 1141141114	1 0111100
lipid_pos.txt	iatom bilayer_index
prot_pos.txt	iatom backbone_index

iatom: atom index starting from 0.

bilayer_index: A (bilayer B1) or B (bilayer B2) backbone_index: BB (backbone) or SC (side chain) Modification of Python scripts for OpenMM.

There are a number of Python scripts provided by Membrane Builder that need to be modified to support V(X) and U(X). In addition, we introduced an in-house Python class, COMReporter, which generates time series of box sizes and COM of the MP on the fly (see omm_comreporter.py at https://github.com/spark-94/BBS.git). Below we show the modifications in omm_restraint.py, omm_readinputs.py, and openmm_run.py.

- omm_restraint.py: V(X) and U(X) are defined using two Python classes CustomExternalForce and CustomCentroidBondForce in OpenMM, respectively. Detailed modifications are given in Table 4.
- omm_readinputs.py: The implementation of V(X) and U(X) in omm_restraints.py requires modifications in this script to process relevant parameters. Two functions, __init__(self) and read(self, inputFiles), in the class, _OpenMMReadInputs(), are modified. Detailed modifications are given in Tables 5 and 6.
- openmm_run.py: Modifications are made to update V(X) from the box size in the restart file at the start of simulation and to use COMR eporter. Detailed modifications are given in Tables 7 and 8.

Modification of input scripts for equilibration and production.

To provide parameter values for V(X) and U(X), and writing frequency of time series of box sizes and MP's COM, lines in Table 9 are added to all simulations inputs (*.inp). The last three lines in Table 9 are parameters for COMR eporter and U(X), which are not needed for the membrane-only BBS.

We note that the case when the target X_{COM} of an embedded MP is located near the bilayer-bilayer boundary, the initial BBS configuration can be generated by pulling of the MP from the ordered phase to the disordered phase by changing the numerical value of XCOM in Table 9 of the MP in a series of simulations with U(X). Although not essential, modifications for on-the-fly generation of the time series of box dimensions and COM of the MP (omm_comreporter.py) have been useful for convenient parameter updates for U(X) and generation of raw data for free energy profile calculations (Park, Levental, Pastor, & Im, 2023; Park, Yeom, Andersen, Pastor, & Im, 2019).

6.2 Verification of lateral packing in BBS

The BBS is designed to preserve the individual bilayer properties except the interface regions (within a distance $X_{\rm M}$ from the simulation box center and boundaries along the X-dimension, see Fig. 1). The restraining potential

Table 4 Additional lines in restraints(system, crd, inputs), in omm_restraint.py.

```
# V(X)
if inputs.fc_wall > 0:
  print("setup BBS restraint: CustomExternalForce")
  fc_wall = input.fc_wall
  # flat-bottom restraints to separate lipid
  wallres = CustomExternalForce('fc wall * (px^2); px = min(0, delta); \
                      delta = r - droff; r = abs(x - x0);')
  wallres.addPerParticleParameter('fc wall', inputs.fc wall)
  wallres.addPerParticleParameter('x0')
  wallres.addPerParticleParameter('droff')
  # read lipid_pos.txt (with additional index , A/B)
  for line in open('restraints/lipid pos.txt', 'r'):
     segments = line.strip().split()
     atom1 = int(segments[0])
     bside = segments[1] # A or B
     if bside == "A":
       x0 = (inputs.wall xref+1.0)* boxlx / 2 # 0.75
       droff = ((1.0-inputs.wall xref)*boxlx)/2 - inputs.margin
       wallres.addParticle(atom1, [fc_wall,x0, droff])
     elif bside == "B":
       x0 = inputs.wall xref / 2 * boxlx # 0.25
       droff = (inputs.wall xref* boxlx) / 2 - inputs.margin
       wallres.addParticle(atom1, [fc_wall,x0, droff])
  system.addForce(wallres)
# U(X) as a function of backbone XCOM
if inputs.fc com > 0:
  print("setup COM res: CustomCentroidBondForce");
  comres = CustomCentroidBondForce(1, "k*(x1-x0)^2")
  comres.addPerBondParameter('k')
  comres.addPerBondParameter('x0')
  k=inputs.fc com
  x0=inputs.com
  particles1=[]
  for line in open('restraints/prot pos.txt', 'r'):
     segments = line.strip().split()
     atom1 = int(segments[0])
     state = segments[1]
     if state == 'BB': particles1.append(atom1) # Choose backbone for COM
  comres.addGroup(particles1)
  comres.addBond([0], [k,x0,y0])
  system.addForce(comres)
```

V(X) (Eq. (1)) does not influence the lateral packing in core bilayer regions; hence the membrane properties would not vary in these regions. Considering this, the lateral packing of bulk phases in a BBS can be verified by comparing their properties with those from individual bilayers.

Table 5 Additional lines in __init__(self) in the class _OpenMMReadInputs() in omm_readinputs.py.

```
# in __init(self)__, parameters are initialized
    self.nstcom
                  = 0
                          # Frequency of writing box size & COM of the MP (steps)
    self.fc wall
                  = 0.0
                          # Force constant for V(X) (kJ/mol/nm^2)
    self.margin
                  = 0.0
                          #XM
                  = 0.0
                          # X-COM restraint
    self.fc com
    self.com
                  = 0.0
                          # X-COM
    self.wall xref = 0.0
                           # Fractional X-coordinate of the B1-B2 interface
```

Table 6 Additional lines in read(self, inputFile) in the class _OpenMMReadInputs() in omm_readinputs.py.

```
# in read(self, inputFile), parameters are read
            if input param == 'NSTCOM':
                                                   self.nstcom
                                                                     = int(input value)
            if input param == 'FC WALL':
                                                   self.fc wall
                                                                     = float(input value)
            if input param == 'FC COM':
                                                   self.fc com
                                                                     = float(input value)
            if input param == 'COM':
                                                                     = float(input_value)
                                                   self.com
            if input param == 'MARGIN':
                                                   self.margin
                                                                     = float(input value)
            if input param == 'WALL XREF':
                                                   self.wall xref
                                                                     = float(input value)
```

For a lipid-only BBS, one can calculate the component APLs and/or deuterium order parameters for the core regions (where the effects of V(X) is negligible). For a MP-including BBS, shell-wise component APLs and/or order parameters for the core region can be calculated, from which the results for the third shell and beyond can be used for the verification. Of course, one can verify the lateral packing using other appropriate properties such as the membrane thicknesses and bond-orientational order parameters (for hexagonal lipid tail packing). When both bilayers are in disordered phases, the ratios of diffusion coefficients (between components in the same and/or other bilayers) can also be uses for the verification. When calculated properties are within statistical uncertainties of those from individual bilayers, the lateral packing of bilayers in the BBS can be regarded as being preserved.

6.3 Examples

Here, we present examples of BBS, which were simulated using conventional or (replica exchange) US MD, depending on the mobility of lipids and partitioning molecule(s).

Table 7 Additional lines in openmm_run.py to update V(X).

```
# At the end of command line block belonging to # Build simulation context
box = simulation.context.getState().getPeriodicBoxVectors()
boxlx = box[0][0].value in unit(nanometers)
for force in simulation.system.getForces():
  if type(force) == CustomExternalForce and force.getPerParticleParameterName(0) ==
'fc wall':
  fc wall = input.fc wall
  break
Natom = force.getNumParticles()
iatom = 0
while iatom < Natom:
  param = force.getParticleParameters(iatom)
  # param=(atom index, [fc wall,x0,droff])
  x0 ref = param[1][1] / boxlx # Xref of each atom
  if x0 ref < inputs.wall xref:
     x0 = inputs.wall xref * boxlx / 2
     droff = (inputs.wall xref * boxlx)/2 - inputs.margin
  if inputs.wall xref < x0 ref:
     x0 = (inputs.wall xref + 1.0) / 2 * boxlx
     droff = (1.0 - inputs.wall xref) * boxlx / 2 - inputs.margin
  force.setParticleParameters(iatom, param[0], [fc_wall,x0, droff])
  iatom += 1
force.updateParametersInContext(simulation.context)
```

Table 8 Additional lines in openmm_run.py to report box sizes and COM of the MP.

```
# In the command line block belonging to # Production
if inputs.nstcom > 0:
if not args.ocom: args.ocom = 'output.com'
simulation.reporters.append(COMReporter(args.ocom, inputs.nstcom))
```

Cholesterol partitioning.

The first example is conventional MD simulations for Chol partitioning between two phase bilayers composed of unsaturated ((1-palmitoyl, 2-oleoylphosphatidylcholine) POPC or DOPC) and saturated lipids (DPPC). To verify convergence, two initial Chol distributions were considered (left panels in Fig. 3A). Differently from the suggested aspect ratio of L_{X} : $L_{Y} = 2:1$, the ratio L_{X} : $L_{Y} = 1:1$ was employed for simulations with CHARMM. In fact, this aspect ratio is better than L_{X} : $L_{Y} = 2:1$ for partitioning of multiple copies of small molecules between two bilayers. Mole fractions for two initial Chol distributions were converged around t = 350 ns (upper panel in Fig. 3B), after the steady-state

Table 9 Additional lines in simulation input files for V(X) and U(X).

```
# 0.5 * kr (kJ/mol/nm^2); ~ 0.5 kcal/mol/A^2
          = 100.0
fc wall
margin
          = 0.2
                      # XM (the half width of mixing zone) (nm)
wall xref = 0.5
                      # Position of the B1-B2 interface in the BBS (fractional LX)
nstcom
          = 500
                      # Frequency of writing box size & com (stpes)
          = 753.15
                      # force constant for U(X) (kJ/mol/nm^2) # there is no 1/2 factor
fc_com
          = XCOM
com
                      # target position for U(X) (nm); substitute XCOM with real value!
```

of the number of interfacial Chol around t=100–200 ns (lower panel in Fig. 3B). The estimate of $K_{\rm p}=1.35\pm0.04$ of Chol between POPC and DOPC from these BBS simulations at $T=318\,\rm K$, agrees excellently with experimentally determined $K_{\rm p}=1.40\pm0.11$ between 1-stearoyl, -2-oleoylphosphocholine (SOPC) and DOPC at the same T, where SOPC is close to POPC.

The insertion free energy of Chol to N-stearoyl-d-sphingomyelin (SSM) and POPC at $T=329\,\mathrm{K}$ from US simulations are $\Delta G(\mathrm{bulk} \to \mathrm{SSM}) = -13.1 \pm 0.4\,\mathrm{kcal/mol}$ and $\Delta G(\mathrm{bulk} \to \mathrm{POPC}) = -12.0 \pm 0.3\,\mathrm{kJ/mol}$, from which the partition free energy of Chol between SSM and POPC is calculated as $\Delta G_{\mathrm{p}}(\mathrm{POPC} \to \mathrm{SSM}) = -1.1 \pm 0.6\,\mathrm{kcal/mol}$ (Zhang et al., 2008). The results clearly show that the uncertainties in the US sampling simulations are accumulated to be comparable to the free energy itself. From our conventional MD simulations, $\Delta G_{\mathrm{p}} = -k_{\mathrm{B}}T\,\mathrm{ln}\,K_{\mathrm{p}}(\mathrm{DOPC} \to \mathrm{POPC}) = -0.19 \pm 0.02\,\mathrm{kcal/mol}$, whose uncertainty is significantly smaller than the magnitude of free energy. The convergence between two initial Chol distributions and excellent agreement of K_{p} between simulation and experiments verify the efficacy of BBS for partitioning of fast diffusing molecules using conventional MD.

Gramicidin A partitioning

The next example is the partitioning of gramicidin A (gA) between DLPC and DMPC bilayers (Fig. 4A), for which US simulations were employed. As shown in the snapshots (Fig. 4B) and analyzed bilayer properties, the DMPC bilayer was less perturbed than the DLPC bilayer, consistent with the previous simulations (Beaven et al., 2017; Kim et al., 2012). The calculated potential of mean force (PMF) profile clearly shows the expected symmetry axes (at X centers of bilayers), which supports the bilayers in the BBS are well controlled (upper panel in Fig. 4C). The transfer free energy, $\Delta G_p = -k_B T \ln K_p(\text{DLPC} \rightarrow \text{DMPC}) = -2.2 \pm 0.7 \text{ kcal/mol}$, which agrees with the previous simulations (Beaven et al., 2017; Kim et al., 2012; Sodt, Beaven, Andersen, Im, & Pastor, 2017) that an effective

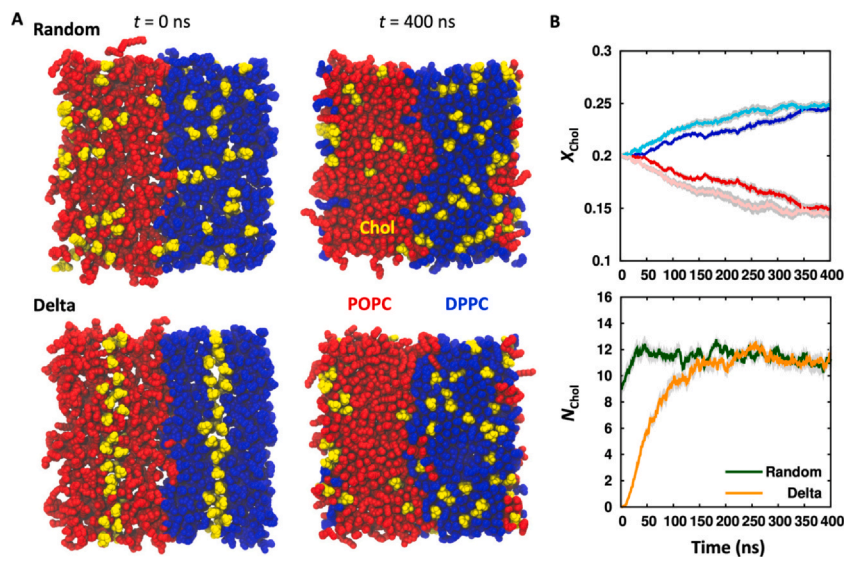


Fig. 3 (A) Snapshots of cholesterol partitioning in a binary bilayer of POPC and DPPC. Two different initial Chol distributions (left column) were simulated for 400 ns (middle column), where Chol mostly partitioned into DPPC bilayer. (B) Time series of Chol mole fraction (X_{Chol} , top) in each bilayer and the number of interfacial Chol (N_{Chol} , bottom) for POPC-DPPC BBS. X_{Chol} in POPC and DPPC bilayers for initial delta Chol distribution are shown in red and blue, whereas those for initial random Chol distribution are shown in pink and cyan. Time series for each initial Chol distribution were averaged over 10 independent simulations, whose standard errors are shown as grey area. Adapted with permission from Reference Park, S., & Im, W. (2018). Quantitative characterization of cholesterol partitioning between binary bilayers. *Journal of Chemical Theory and Computation*, 14(6), 2829–2833, https://doi.org/10.1021/acs.jctc.8b00140. Copyright 2018 American Chemical Society.

hydrophobic thickness of gA ~26 Å better explains the bilayer deformation and continuum model rather than ~22 Å from its structure. The calculated PMF profile can be well modeled by a free energy composed of contributions from the bilayer deformation, restraining potentials, and line tension at the bilayer-bilayer interface (lower panel in Fig. 4C).

LAT TM partition free energy in Lo-Ld BBS.

The preceding examples can be considered as proof-of-concept simulations for the application to the MP partitioning between Lo and Ld phases. In the example below, we have simulated all-atom models of the Lo-Ld BBS, which are composed of Lo and Ld phase bilayers consisting of DSPC, POPC, and Chol with an embedded TM of linker for activation of T-cell (LAT TM). Two sets of Lo and Ld compositions close to those at

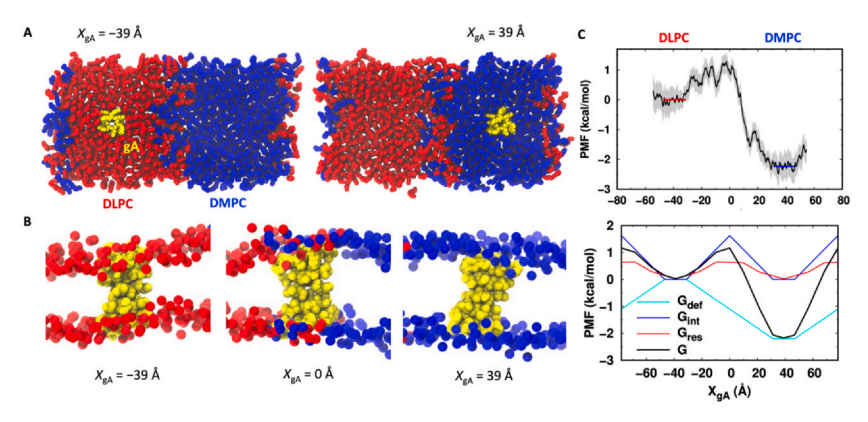


Fig. 4 (A) Snapshots of gA in a BBS of DLPC and DMPC from US simulations at t=360 ns. The hydrophobic tails of DLPC and DMPC are shown in red and blue, respectively, and gA are shown in yellow. The hydrogen and other components are omitted for clarity. (B) Lipid adaptation to gA at $X_{\rm gA}=-39$ A, $X_{\rm gA}=0$ Å, and $X_{\rm gA}=39$ Å at t=360 ns. For clarity only the first carbon in the hydrophobic tails and gA are shown. (C) The PMF profiles from US simulations of gA in DLPC-DMPC BBS from the last 300 ns trajectories (top) and that from a model for gA-lipid interactions in the BBS (*G*), composed of the contributions from the bilayer deformation ($G_{\rm def}$), the line tension at the bilayer-bilayer interfaces ($G_{\rm int}$), and the binary bilayer restraining potential ($G_{\rm res}$) (bottom). Adapted with permission from Reference Park, S., Yeom, M. S., Andersen, O. S., Pastor, R. W., & Im, W. (2019). Quantitative characterization of protein-lipid interactions by free energy simulation between binary bilayers. *Journal of Chemical Theory and Computation*, *15*(11), 6491–6503, https://doi.org/10.1021/acs.jctc.9b00815. Copyright 2019 American Chemical Society.

high- and low-Chol tie-lines in ternary phase diagram were considered and the LAT TM was either wild type or depalmitoylated. Replica exchange US (REUS) simulations are employed for better sampling, where each window was simulated for 4.5 µs as necessitated by slow diffusion in Lo phases. From the simulations, POPC enrichment around the LAT TM in the Lo phase was observed (Fig. 5A and B), which has not been observed in the previous CG simulations of phase separated ternary bilayers (Kwon, Pantelopulos, & Straub, 2023; Lin et al., 2018; Lorent et al., 2017), where unsaturated lipids are almost exclusively present in the Ld-phase. Moreover, the available models for raft affinity of MPs do not take the detailed organization of Lo-phase structures into account (Lorent et al., 2017). The observed enrichment of unsaturated lipids around the LAT TM clearly demonstrates the importance of the detailed Lo-phase structures and the role of unsaturated lipids in Lo-phase partitioning of MP. However, the calculated PMF profiles from the last 3-µs trajectories (Fig. 5C) still have large statistical uncertainties, and the LAT TM does not show the Lo-phase

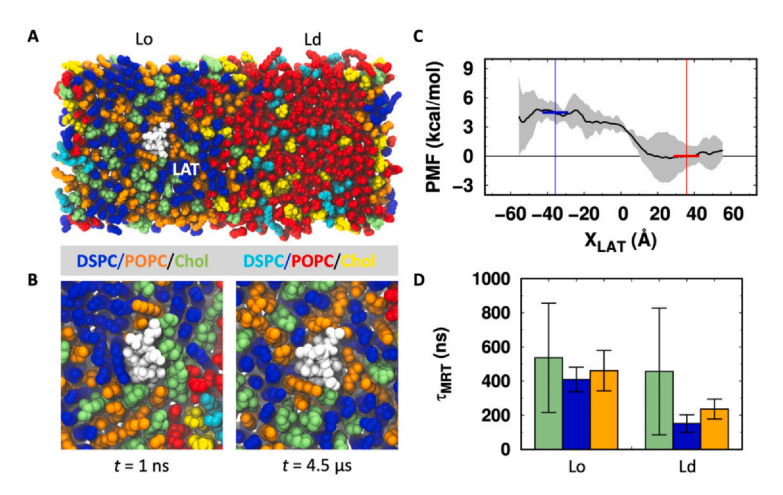


Fig. 5 (A) Snapshots of Lo-Ld BBS composed of DSPC, POPC, and Chol with an embedded wild-type LAT TM (LATWT) from REUS simulations at $t = 4.5 \mu s$. The Lo-Ld phase lipid compositions are chosen close to the high-Chol tie-line compositions (Konyakhina, Wu, Mastroianni, Heberle, & Feigenson, 2013; Usery et al., 2018). (B) Lipid distributions around the LAT TM at t = 1 ns and at $t = 4.5 \,\mu s$ for the same replica. (C) The PMF profile of LAT^{WT} in the high-Chol Lo-Ld BBS as a function of X_{LAT} using the last 3-µs trajectories from REUS simulations. The partition free energy is estimated as the difference between the average PMFs over two plateaus (blue and red). The 95% confidence interval (CI) from three 1-µs block PMF profiles are shown as the grey area. (D) The mean residence time (τ_{MRT}) of lipid type in the high-Chol Lo-Ld BBS. τ_{MRT} for DSPC, POPC, and Chol are shown in blue, orange, and lime, respectively. The error bars are the 95% CI from the replicas assigned to Lo and Ld phases. Adapted with permission from Reference Park, S., Levental, I., Pastor, R. W., & Im, W. (2023). Unsaturated lipids facilitate partitioning of transmembrane peptides into the liquid ordered phase. Journal of Chemical Theory and Computation, 19(15), 5303-5314, https://pubs.acs.org/doi/10.1021/acs.jctc.3c00398. Copyright 2023 American Chemical Society. Further permissions related to the material excerpted should be directed to the ACS.

affinity in agreement with the experiments in GUVs (Bacia et al., 2004; Kahya et al., 2005; Shogomori et al., 2005) and previous CG US simulations (Kwon et al., 2023; Lin et al., 2018; Lorent et al., 2017). The results in turn suggest that more complex compositions may be necessary to model rafts in cell membranes. The large uncertainties in the PMF profiles and long mean residence time of lipids in the first shell around the LAT TM (Fig. 5D) indicate the difficulty in the sampling of Lo phases.

6.4 Parameter tuning

In the BBS, there are a number of parameters that can be tuned for better performance. The aspect ratio, $L_X:L_Y$, is the parameter related to the shape

of the BBS, which is set to be 2:1 for a BBS with an embedded MP. This ratio is a natural choice given the requirement that a BBS includes at least the first three lipid shells around the MP (Eq. (4a)). However, different $L_X:L_Y$ can be set for other situations. For example, a BBS with a smaller aspect ratio, $L_X:L_Y=1:1$, was employed for Chol partitioning, which is advantageous for direct partitioning of multiple copies of fast diffusing molecules. When one is interested in the interface of a large Lo phase with a radius of R ($\gg L_Y$) surrounded by the Ld phase, one can consider a BBS with $L_X=2R$ with a large X_M and/or smaller k_r for wider mixing zones (see Fig. 1 and Eq. (1)). For this BBS, the ratio of interface length and Lophase SA, $4/L_X$, matches with that of the discoidal Lo phase, 2/R.

Regarding the restraining potential, V(X), there are two adjustable parameters, $k_{\rm r}$ and $X_{\rm M}$, which are set to be $k_{\rm r} = 200\,{\rm kJ/mol/nm^2}$ (or 0.5 kcal/mol/Ų) and $X_{\rm M} = 8\,{\rm Å}$. Current values of $k_{\rm r}$ and $X_{\rm M}$ are chosen so that the lateral packing of individual bilayers can be adjusted within a few lipid layers along the X-dimension. Depending on the required sharpness and ruggedness of the bilayer-bilayer interfaces, $k_{\rm r}$ and $X_{\rm M}$ can be adjusted based on Eqs. (3) and (4). The update frequency of V(X) is an additional parameter, which is set to be 1 ns in our work. This is an empirical choice to reduce overhead from frequent restarts.

6.5 What can go wrong?

Although we designed a BBS to minimize artifacts related to the system size and lateral packing (see above), these may persist in the BBS, especially, when the system size is not sufficiently large and/or SAs of individual bilayers are significantly mismatched. Aside from the visual inspection of simulation trajectories, these issues can be detected by monitoring the fraction of restrained lipids (f_{res}), the restraining energy (E_{res}), and the lipid density profiles along the X-dimension ($\propto p(X)$). Artifacts in the lateral packing can also be found by monitoring (shell-wise) component APLs and order parameters.

Large f_{res} is indicative of small system size as it is inversely proportional to L_X (Eq. (3a)). In addition, it is associated with high restraining energy, E_{res} . Considering an acceptable restraining energy in each bilayer is $\sim k_B T$, one can find a criterion, $f_{res} \leq f_{max} = 4/N_{tot}$ (Eq. (3d)), where N_{tot} is the total number of lipids in the BBS. Whenever the observed f_{res} is significantly larger than f_{max} , one needs to consider a larger BBS (by a factor of $(f_{res}/f_{max})^{1/2}$ to each X and Y dimension) or a larger aspect ratio, $L_X:L_Y$, providing that adjusted L_Y satisfies the criterion given by Eq. 5.

Significant discrepancies in component APLs between the core region (excluding the mixing zone) and those from the corresponding symmetric bilayer indicate that the lateral packing is poorly controlled. This artifact may arise in a BBS with strong V(X) and narrow mixing zones (large k_r and small X_M , see Eq. (1)), indicating that component APLs are poorly estimated or the area of mixing zones is significantly smaller than that of the MP (see Eq. (4b)). Once the lateral packing issue is detected, one can lower k_r and/or increase X_M to allow wider mixing zones. However, care should be taken because $d_{\rm res} + X_M < L_X/4$ must be satisfied for the BBS with a wider core region than mixing zones. When the system size is small or bilayer-bilayer interfaces are required to be sharp and even, this adjustment may not be applied. A cleaner solution is to start with better SA matched bilayers for the generation of BBS.

Although it is not an artifact in the BBS generation, the mobility of lipids and MP in the ordered phase can be an issue in conventional MD simulations. Considering finite size effects in membranes (Camley, Lerner, Pastor, & Brown, 2015; Venable et al., 2017) and diffusion under confinement (Bocquet & Barrat, 1995), increasing system size can increase the diffusivity. However, this cannot accelerate diffusion more than the thermodynamic limit. Hence, once slow diffusion is detected, one needs to consider additional help from some free energy methods, for example, US or REUS.

7. Performance

The BBS simulation method is straightforward and can be implemented in the script level for any MD package that supports the BBS restraining potential, V(X). Here, we provide a concise summary of advantages and limitations of the BBS simulation method.

7.1 Advantages

The most distinct advantage is the flexibility of the BBS configuration, where each leaflet in each bilayer can have different lipid compositions in different phases. This flexibility arises from the applied V(X), which prevents bilayer mixing and allows crisp bilayer-bilayer interfaces. Due to well-maintained interfaces, conventional MD can be applied for partitioning of fast diffusing molecules between two phases. Another advantage is that the BBS can be generated with a significantly smaller system-size for separated phases (Park et al., 2023) than the critical size required for macroscopic phase separation. From our estimate (Eq. (5)), a leaflet in a BBS with a small

embedded TM is composed of less than 120 lipids (less than 480 lipids in total), which is less than ~32% of the critical size of ~1500 lipids for CG ternary bilayer of DPPC, DIPC, and Chol (Pantelopulos et al., 2017). Lastly, the BBS can be simulated using all available methods supported by MD packages including those used in examples above.

7.2 Limitations

Although the BBS is designed to preserve membrane properties as described in **Binary bilayer system** and **Implementation**, artifacts from poorly estimated component APLs and/or system-size cannot always be remedied only by parameter tuning. Thus, care must be taken in the calculation of component APLs from preliminary symmetric bilayer simulations. In the current implementation, compositions of the two phases are fixed; that is, the phases are in "mechanical", but not in "chemical", equilibrium. If the predetermined compositions are poorly chosen (e.g., not in the same tie line), the BBS would simulate phases that would not normally coexist. Hence, the compositions should be chosen as accurately as possible. The slow diffusion in ordered phases cannot be increased arbitrarily beyond the thermodynamic limit just by increasing the system size. Hence the application to an all-atom model of coexisting ordered-disordered phases to calculate ΔG_p still remains difficult due to long time scales even using available free energy methods.

8. Alternatives

The conventional approaches for the calculation of K_p (or $\Delta G_p = -k_B T \ln K_p$) of a MP can be either a set of insertion free energy simulations (Bereau et al., 2015; Lopez et al., 2013; Zhang et al., 2008) or direct US simulations in phase separated mixed bilayers (Lin et al., 2018; Lorent et al., 2017). For structurally similar MPs, the ratio of K_p 's (i.e., relative partition free energy) can be calculated from alchemical free energy simulations (Gumbart & Roux, 2012). Below, we discuss these approaches and their limitations.

In the indirect insertion free energy method, a set of insertion free energies of the MP, $\Delta G(RM \to B1)$ and $\Delta G(RM \to B2)$ are calculated from independent US simulations of bilayers B1 and B2, respectively, where RM is a reference medium, for example, bulk solvent or β -CD. The partition free energy, $\Delta G_p(B1 \to B2)$ is then obtained from the thermodynamic cycle as $\Delta G_p(B1 \to B2) = \Delta G(RM \to B2) - \Delta G(RM \to B1)$. Unlike the success of the indirect approach in experiments of Chol

partitioning between β -CD and vesicles due to the large signal to noise ratio from the high Chol exchange rate (Leventis & Silvius, 2001; Niu et al., 2002; Ohvo-Rekilä et al., 2000), the situation is opposite in computational approaches: Uncertainties from two US simulations accumulate and thus lower the precision of the indirectly estimated ΔG_p . Also, this approach requires a reference medium and a large number of windows along the membrane normal from the bilayer center to the reference medium, hence it is computationally intensive in general. For the calculation of K_p (or ΔG_p) of fast diffusing molecules between two phases, the conventional MD of BBS can be a good choice due to sufficiently high exchange rate of the partitioning molecules between two phases and less computational cost.

In the direct US simulation approach, $\Delta G_p(B1 \rightarrow B2)$ is calculated as $\Delta G_{\rm p}$ (B1 \rightarrow B2) = $\langle G_{\rm B2} \rangle - \langle G_{\rm B1} \rangle$, where $\langle G_{\rm Bi} \rangle$ is the average PMFs for the central plateau in the bilayer Bi. To apply this approach two bilayers B1 and B2 should be phase separated, and thus it cannot be applied for the partitioning between two disordered phases. Considering the large system size (>1500 lipids) required for macroscopic phase separation, the direct US simulation approach would be even more computationally intensive than the indirect free energy approach. Moreover, it was observed that the phase boundary can be significantly distorted (Kwon et al., 2023). The distorted interface in turn significantly affects the calculated PMF profiles due to accumulated energetic penalty associated with it, shown as the disappearance of the flat region in the ordered phase. To maintain the plateau, the system size should be even larger so that the core region in the ordered phase is free of the interface effects. Therefore the BBS is clearly better suited for direct US simulations, which can preserve the bulk phase properties in a significantly smaller binary bilayer with even phase boundaries due to the applied V(X) (Kwon et al., 2023; Park et al., 2023).

In the alchemical free energy approach, one calculates the free energy difference, $\Delta\Delta G_{\rm p}({\rm M1} \to {\rm M2})~(=-k_{\rm B}T \ln[K_{\rm p}({\rm M2})/K_{\rm p}({\rm M1})])$ between two structurally similar molecules or MPs indirectly from a set of alchemical free energy simulations, M1 \to M2, in the membrane and bulk, where M1 and M2 are two molecules of interest. Like the insertion free energy approach, this approach is computationally intensive and prone to the accumulated uncertainties due to the requirement of a reference medium. Moreover, due to the limitations in the method itself, its applicability is limited to the relative partitioning of two structurally similar molecules. The insertion free energy approach or a set of two BBS simulations can be applied in this case to indirectly calculate the ratio of $K_{\rm p}$'s.

9. Outlook

Simulation approaches for the partitioning provide detailed interactions between components as well as membrane structures, from which valuable insights into underlying physical mechanisms can be obtained. However, the quality of calculated K_p (and ΔG_p) values from the available free energy and BBS methods depends on the quality of the sampling. As always, insufficient sampling results in poor estimates with large uncertainties, which are more severe in ordered phases due to the lower mobility of lipids and MPs than disordered phases. As the detailed structures in the Lo phases are shown to be important features in the MP's partitioning (Park et al., 2023), the sampling of a well-equilibrated ordered phase is essential. Hence, significant efforts need to be made to enhance sampling of ordered phases.

Methods for efficient lipid swapping would enhance sampling in ordered phases. One conceivable approach is based on the Monte Carlo method, where a trial lipid swap is accepted or declined according to the Metropolis criterion. The trial swap may be a series of inflation, swapping, and deflation, which is analogous to the algorithm used for the insertion of a MP (Kandt, Ash, & Peter Tieleman, 2007; Schmidt & Kandt, 2012). This trial may be also performed by an alchemical swapping of lipid pairs, which was developed and applied to calculate the exchange free energies of unsaturated and saturated lipids in Lo and Ld phases (Bennett et al., 2018). By combination with this type of enhanced swapping methods, efficient sampling of membrane configurations would be allowed, thereby improving both the precision and accuracy of K_p .

Raft affinity of MPs is biologically important but has not been well studied by computational methods. One obvious difficulty is the requirement of large system size to have a representative piece of a raft, where the phase separation would be transient with diffuse interfaces. Another difficulty arises from the fact that the raft composition might well depend on the presence of the raft proteins, in the sense that these proteins are not passive environment seekers but actively contribute to the phase separation. In this case, the notion of a pre-existing phase contrasts from where a raft protein picks a preferred side could be misleading and the phase separation might not occur without proteins.

So far ternary lipid models have been used in simulations for the partitioning of MPs between Lo and Ld phases, whose results (Kwon et al., 2023; Lin et al., 2018; Lorent et al., 2017; Park et al., 2023) agree with those from GUV experiments (Bacia et al., 2004; Kahya et al., 2005; Shogomori et al., 2005), suggesting that ternary models of membrane may not be sufficient to

model cell membranes. Besides the compositional complexity, it has been known that the difference between ordered and disordered phases in GPMVs is significantly smaller than that in typical sizes of GUVs in experiments, suggesting that these phases are close to the critical point in the phase diagram (Kaiser et al., 2009; Machta, Veatch, & Sethna, 2012; Sezgin et al., 2012; Steinkühler, Sezgin, Urbančič, Eggeling, & Dimova, 2019; Veatch, Soubias, Keller, & Gawrisch, 2007). Thus, to model rafts, it is necessary to consider high tie-line Lo-Ld compositions near the critical point, which remains difficult in conventional bilayer simulations.

The BBS is well-suited for the co-existing Lo-Ld phases near the critical point, where these phases are well-maintained due to V(X) (Eq. (1)) in rather small systems (see **Determination of lateral dimensions** in **Implementation**). Thus the system-size issue can be easily resolved in a sufficiently large BBS where the Lo phase has a few isolated clusters of hexagonally packed saturated lipids surrounded by unsaturated lipids and Chol (see Fig. 5A). In addition, the BBS allows a direct monitoring how MP can influence the Lo phase, for example, the recruitment of unsaturated lipids around proteins without significant perturbation of tightly packed saturated lipids (Park et al., 2023). Hence, with a better designed membrane model for the raft, the BBS could be a valuable platform for the raft affinity of MPs.

Besides the partitioning in bilayer phases, the BBS structure can be readily extended for the partitioning in various environments. For example, the binary monolayer system can be readily prepared for the partitioning within monolayer phases. Individual monolayer systems can be easily prepared by CHARMM-GUI *Membrane Builder*, from which a binary monolayer system can be easily prepared following the generation procedure of the BBS. Partitioning of surfactant proteins in pulmonary Lc- and Le-phase monolayers, important in the pulmonary surfactant function, then can be determined. In addition, the small molecule distribution between water and organic solvents can be easily simulated using the binary phase system (i.e., calculation of the distribution coefficient, log *D*), which has been a topic in SAMPL challenge since SAMPL5 (Mobley, 2016). Conventional MD can be employed for log *D* calculations.

10. Connections

The following chapters in this volume set are especially relevant to the present topic:

- Characterization of domain formation in complex membranes: Analyzing the bending modulus from simulations of complex membranes, Trollmann, M.F.W., & Böckmann, R.A. In this chapter, Getis-Ord Statistics for domains in membranes and the development of hidden Markov Models from local information on area per lipid and the tail order parameter are discussed. These can be applied to analyze bilayers in the BBS.
- Modeling Asymmetric Cell Membranes at All-atom Resolution, Bodosa, J., Pane, A.J., & Klauda, J.B. This chapter describes numerous methods for generating asymmetric membranes, which can be used to generate (asymmetric) bilayer patches in the BBS.
- Building complex membranes with Martini 3, Ozturk et al. This chapter
 describes generation of coarse-grained membranes with Martini 3, which
 can be applied to the generation of bilayer patches in the coarse-grained
 model of BBS.
- Characterizing local order and packing in co-existing fluid phase membranes in molecular simulations using non-affine parameter and 3D packing defects, Tripathy, M., & Srivastava, A. This chapter describes a method to identify domains by affine deformation of lipids. The properties of bilayer patches in the BBS can also be analyzed using their methods.
- Simulating asymmetric membranes using P2₁ periodic boundary conditions, Rice, A. & Pastor, R.W. This chapter describes how P2₁ simulations can be used to generate asymmetric bilayers in chemical equilibrium between leaflets. Hence, P2₁ equilibration can be considered for the generation of asymmetric bilayer patches in the BBS.

Acknowledgements

This research was supported by NSF MCB-2111728, NIH R01 GM138472 (to W.I.), the Intramural Research Program of the NIH, the National Heart, Lung, and Blood Institute, and the use of the high-performance computational capabilities at the National Institutes of Health, Bethesda, MD (NHLBI LoBoS cluster) (to R.W.P.). We thank Markus Deserno for his careful reading and very helpful suggestions.

References

- Abraham, M. J., Murtola, T., Schulz, R., Páll, S., Smith, J. C., Hess, B., & Lindah, E. (2015). Gromacs: High performance molecular simulations through multi-level parallelism from laptops to supercomputers. *SoftwareX*, 1–2, 19–25.
- Åqvist, J., Wennerström, P., Nervall, M., Bjelic, S., & Brandsdal, B. O. (2004). Molecular dynamics simulations of water and biomolecules wit a Monte Carlo constant pressure algorithm. *Chemical Physics Letters*, 384(4–6), 288–294.
- Bacia, K., Schuette, C. G., Kahya, N., Jahn, R., & Schwille, P. (2004). SNAREs prefer liquid-disordered over "raft" (liquid-ordered) domains when reconstituted into giant unilamellar vesicles. *Journal of Biological Chemistry*, 279(36), 37951–37955.

- Beaven, A. H., Maer, A. M., Sodt, A. J., Rui, H., Pastor, R. W., Andersen, O. S., & Im, W. (2017). Gramicidin a channel formation induces local lipid redistribution I: Experiment and simulation. *Biophysical Journal*, 112(6), 1185–1197.
- Bennett, W. F. D., Shea, J. E., & Tieleman, D. P. (2018). Phospholipid chain interactions with cholesterol drive domain formation in lipid membranes. *Biophysical Journal*, 114(11), 2595–2605.
- Bereau, T., Bennett, W. F. D., Pfaendtner, J., Deserno, M., & Karttunen, M. (2015). Folding and insertion thermodynamics of the transmembrane WALP peptide. *Journal of Chemical Physics*, 143(24), 243127.
- Bocquet, L., & Barrat, J.-L. (1995). Diffusive motion in confined fluids: Mode-Coupling results and molecular-dynamics calculations. *Europhysics Letters*, 31(8), 455–460.
- Bonomi, M., Branduardi, D., Bussi, G., Camilloni, C., Provasi, D., Raiteri, P., ... Parrinello, M. (2009). PLUMED: A portable plugin for free-energy calculations with molecular dynamics. *Computer Physics Communications*, 180(10), 1961–1972.
- Brooks, B. R., Brooks, C. L., Mackerell, A. D., Nilsson, L., Petrella, R. J., Roux, B., ... Karplus, M. (2009). CHARMM: The biomolecular simulation program. *Journal of Computational Chemistry*, 30(10), 1545–1614.
- Camley, B. A., Lerner, M. G., Pastor, R. W., & Brown, F. L. H. (2015). Strong influence of periodic boundary conditions on lateral diffusion in lipid bilayer membranes. *The Journal of Chemical Physics*, 143(24), 243113.
- Casals, C., & Cañadas, O. (2012). Role of lipid ordered/disordered phase coexistence in pulmonary surfactant function. *Biochimica et Biophysica Acta Biomembranes*, 1818(11), 2550–2562.
- Chow, K. H., & Ferguson, D. M. (1995). Isothermal-isobaric molecular dynamics simulations with Monte Carlo volume sampling. *Computer Physics Communications*, 91(1–3), 283–289.
- Diaz-Rohrer, B. B., Levental, K. R., Simons, K., & Levental, I. (2014). Membrane raft association is a determinant of plasma membrane localization. *Proceedings of the National Academy of Sciences of the United States of America*, 111(23), 8500–8505.
- Dolan, E. A., Venable, R. M., Pastor, R. W., & Brooks, B. R. (2002). Simulations of membranes and other interfacial systems using P21 and Pc periodic boundary conditions. *Biophysical Journal*, 82(5), 2317–2325.
- Durell, S. R., Brooks, B. R., & Bennaim, A. (1994). Solvent-Induced forces between two hydrophilic groups. *Journal of Physical Chemistry*, 98(8), 2198–2202.
- Eastman, P., Swails, J., Chodera, J. D., McGibbon, R. T., Zhao, Y. T., Beauchamp, K. A., ... Pande, V. S. (2017). OpenMM 7: Rapid development of high performance algorithms for molecular dynamics. *PLoS Computational Biology*, 13(7), e1005659.
- Essmann, U., Perera, L., Berkowitz, M. L., Darden, T., Lee, H., & Pedersen, L. G. (1995). A smooth particle mesh Ewald method. *Journal of Chemical Physics*, 103(19), 8577–8593.
- Feigenson, G. W. (2009). Phase diagrams and lipid domains in multicomponent lipid bilayer mixtures. *Biochimica et Biophysica Acta, Biomembranes, 1788*(1), 47–52.
- Fiorin, G., Klein, M. L., & Hénin, J. (2013). Using collective variables to drive molecular dynamics simulations. *Molecular Physics*, 111(22–23), 3345–3362.
- Gao, Y., Lee, J., Smith, I. P. S., Lee, H., Kim, S., Qi, Y., ... Im, W. (2021). CHARMM-GUI supports hydrogen mass repartitioning and different protonation states of phosphates in lipopolysaccharides. *Journal of Chemical Information and Modeling*, 61(2), 831–839.
- Guixà-González, R., Rodriguez-Espigares, I., Ramírez-Anguita, J. M., Carrió-Gaspar, P., Martinez-Seara, H., Giorgino, T., & Selent, J. (2014). MEMBPLUGIN: Studying membrane complexity in VMD. Bioinformatics (Oxford, England), 30(10), 1478–1480.
- Gumbart, J., & Roux, B. (2012). Determination of membrane-insertion free energies by molecular dynamics simulations. *Biophysical Journal*, 102(4), 795–801.

- Hopkins, C. W., Le Grand, S., Walker, R. C., & Roitberg, A. E. (2015). Long-Time-Step molecular dynamics through hydrogen mass repartitioning. *Journal of Chemical Theory and Computation*, 11(4), 1864–1874.
- Huang, J., & Mackerell, A. D. (2013). CHARMM36 all-atom additive protein force field: Validation based on comparison to NMR data. *Journal of Computational Chemistry*, 34(25), 2135–2145.
- Humphrey, W., Dalke, A., & Schulten, K. (1996). VMD: Visual molecular dynamics. *Journal of Molecular Graphics*, 14(1), 33–38.
- Jo, S., Kim, T., & Im, W. (2007). Automated builder and database of Protein/Membrane complexes for molecular dynamics simulations. *PLoS One*, 2(9), e880.
- Jo, S., Kim, T., Iyer, V. G., & Im, W. (2008). Software news and updates—CHARNIM-GUI: A web-based grraphical user interface for CHARMM. *Journal of Computational Chemistry*, 29(11), 1859–1865.
- Jo, S., Lim, J. B., Klauda, J. B., & Im, W. (2009). CHARMM-GUI membrane builder for mixed bilayers and its application to yeast membranes. *Biophysical Journal*, 97(1), 50–58.
- Jorgensen, W. L., Chandrasekhar, J., Madura, J. D., Impey, R. W., & Klein, M. L. (1983). Comparison of Simple potential functions for simulating liquid water. *Journal of Chemical Physics*, 79(2), 926–935.
- Kahya, N., Brown, D. A., & Schwille, P. (2005). Raft partitioning and dynamic behavior of human placental alkaline phosphatase in giant unilamellar vesicles. *Biochemistry*, 44(20), 7479–7489.
- Kaiser, H. J., Lingwood, D., Levental, I., Sampaio, J. L., Kalvodova, L., Rajendran, L., & Simons, K. (2009). Order of lipid phases in model and plasma membranes. *Proceedings of the National Academy of Sciences of the United States of America*, 106(39), 16645–16650.
- Kandt, C., Ash, W. L., & Peter Tieleman, D. (2007). Setting up and running molecular dynamics simulations of membrane proteins. Methods (San Diego, Calif.), 41(4), 475–488.
- Kim, T., Lee, K. I., Morris, P., Pastor, R. W., Andersen, O. S., & Im, W. (2012). Influence of hydrophobic mismatch on structures and dynamics of gramicidin a and lipid bilayers. *Biophysical Journal*, 102(7), 1551–1560.
- Klauda, J. B., Venable, R. M., Freites, J. A., O'Connor, J. W., Tobias, D. J., Mondragon-Ramirez, C., ... Pastor, R. W. (2010). Update of the CHARMM all-atom additive force field for lipids: Validation on six lipid types. *Journal of Physical Chemistry B*, 114(23), 7830–7843.
- Konyakhina, T. M., Wu, J., Mastroianni, J. D., Heberle, F. A., & Feigenson, G. W. (2013). Phase diagram of a 4-component lipid mixture: DSPC/DOPC/POPC/chol. *Biochimica et Biophysica Acta, Biomembranes*, 1828(9), 2204–2214.
- Kwon, S., Pantelopulos, G. A., & Straub, J. E. (2023). Efficient calculation of the free energy for protein partitioning using restraining potentials. *Biophysical Journal*, 122(11), 1914–1925.
- Lee, J., Patel, D. S., Ståhle, J., Park, S. J., Kern, N. R., Kim, S., ... Im, W. (2019). CHARMM-GUI membrane builder for complex biological membrane simulations with glycolipids and lipoglycans. *Journal of Chemical Theory and Computation*, 15(1), 775–786.
- Levental, İ., Lingwood, D., Grzybek, M., Coskun, Ü., & Simons, K. (2010). Palmitoylation regulates raft affinity for the majority of integral raft proteins. Proceedings of the National Academy of Sciences of the United States of America, 107(51), 22050–22054.
- Leventis, R., & Silvius, J. R. (2001). Use of cyclodextrins to monitor transbilayer movement and differential lipid affinities of cholesterol. *Biophysical Journal*, 81(4), 2257–2267.
- Lin, X., Gorfe, A. A., & Levental, I. (2018). Protein Partitioning into ordered membrane domains: Insights from simulations. *Biophysical Journal*, 114, 1936–1944.
- Lopez, C. A., de Vries, A. H., & Marrink, S. J. (2013). Computational microscopy of cyclodextrin mediated cholesterol extraction from lipid model membranes. *Scientific Reports*, 3, 2071.

- Lorent, J. H., Diaz-Rohrer, B., Lin, X., Spring, K., Gorfe, A. A., Levental, K. R., & Levental, I. (2017). Structural determinants and functional consequences of protein affinity for membrane rafts. *Nature Communications*, 8(1), 1219.
- Lukat, G., Krüger, J., & Sommer, B. (2013). APL@Voro: A voronoi-based membrane analysis tool for GROMACS trajectories. *Journal of Chemical Information and Modeling*, 53(11), 2908–2925.
- Machta, B. B., Veatch, S. L., & Sethna, J. P. (2012). Critical Casimir forces in cellular membranes. *Physical Review Letters*, 109(13).
- Mobley, D. L. (2016). Special Issue: Distribution coefficient prediction: The SAMPL5 challenge—Part 1 of 2. Journal of Computer-Aided Molecular Design, 30.
- Neria, E., Fischer, S., & Karplus, M. (1996). Simulation of activation free energies in molecular systems. *Journal of Chemical Physics*, 105(5), 1902–1921.
- Niu, S. L., Mitchell, D. C., & Litman, B. J. (2002). Manipulation of cholesterol levels in rod disk membranes by methyl-beta-cyclodextrin: Effects on receptor activation. *Journal of Biological Chemistry*, 277(23), 20139–20145.
- Ohvo-Rekilä, H., Åkerlund, B., & Slotte, J. P. (2000). Cyclodextrin-catalyzed extraction of fluorescent sterols from monolayer membranes and small unilamellar vesicles. *Chemistry* and Physics of Lipids, 105(2), 167–178.
- Pandit, S. A., Vasudevan, S., Chiu, S. W., Mashl, R. J., Jakobsson, E., & Scott, H. L. (2004). Sphingomyelin-cholesterol domains in phospholipid membranes: Atomistic simulation. *Biophysical Journal*, 87(2), 1092–1100.
- Pantelopulos, G. A., Nagai, T., Bandara, A., Panahi, A., & Straub, J. E. (2017). Critical size dependence of domain formation observed in coarse-grained simulations of bilayers composed of ternary lipid mixtures. *Journal of Chemical Physics*, 147(9), 095101.
- Park, S., & Im, W. (2018). Quantitative characterization of cholesterol partitioning between binary bilayers. *Journal of Chemical Theory and Computation*, 14(6), 2829–2833.
- Park, S., Levental, I., Pastor, R. W., & Im, W. (2023). Unsaturated lipids facilitate partitioning of transmembrane peptides into the liquid ordered phase. *Journal of Chemical Theory and Computation*, 19(15), 5303–5314.
- Park, S., Yeom, M. S., Andersen, O. S., Pastor, R. W., & Im, W. (2019). Quantitative characterization of protein-lipid interactions by free energy simulation between binary bilayers. *Journal of Chemical Theory and Computation*, 15(11), 6491–6503.
- Parra, E., & Pérez-Gil, J. (2015). Composition, structure and mechanical properties define performance of pulmonary surfactant membranes and films. *Chemistry and Physics of Lipids*, 185, 153–175.
- Phillips, J. C., Hardy, D. J., Maia, J. D. C., Stone, J. E., Ribeiro, J. V., Bernardi, R. C., ... Tajkhorshid, E. (2020). Scalable molecular dynamics on CPU and GPU architectures with NAMD. *Journal of Chemical Physics*, 153(4), 44130.
- Pike, L. J. (2006). Rafts defined: A report on the Keystone symposium on lipid rafts and cell function. *Journal of Lipid Research*, 47(7), 1597–1598.
- Ryckaert, J. P., Ciccotti, G., & Berendsen, H. J. C. (1977). Numerical integration of the cartesian equations of motion of a system with constraints: Molecular dynamics of nalkanes. *Journal of Computational Physics*, 23(3), 327–341.
- Schmidt, T. H., & Kandt, C. (2012). LAMBADA and InflateGRO2: Efficient membrane alignment and insertion of membrane proteins for molecular dynamics simulations. *Journal of Chemical Information and Modeling*, 52(10), 2657–2669.
- Sezgin, E., Kaiser, H. J., Baumgart, T., Schwille, P., Simons, K., & Levental, I. (2012). Elucidating membrane structure and protein behavior using giant plasma membrane vesicles. *Nature Protocols*, 7(6), 1042–1051.
- Sezgin, E., Levental, I., Mayor, S., & Eggeling, C. (2017). The mystery of membrane organization: Composition, regulation and roles of lipid rafts. *Nature Reviews. Molecular Cell Biology*, 18(6), 361–374.

- Shaw, D. E., Grossman, J. P., Bank, J. A., Batson, B., Butts, J. A., Chao, J. C., ... Young, C. (2014). Anton 2: Raising the bar for performance and programmability in a special-purpose molecular dynamics supercomputer. SC '14: Preceedings of the International Conference for High Performance Computing, Networking, Storage and Analysis, SC, 41–53.
- Shogomori, H., Hammond, A. T., Ostermeyer-Fay, A. G., Barr, D. J., Feigenson, G. W., London, E., & Brown, D. A. (2005). Palmitoylation and intracellular domain interactions both contribute to raft targeting of linker for activation of T cells. *Journal of Biological Chemistry*, 280(19), 18931–18942.
- Sodt, A. J., Beaven, A. H., Andersen, O. S., Im, W., & Pastor, R. W. (2017). Gramicidin a channel formation induces local lipid redistribution II: A 3D continuum elastic model. *Biophysical Journal*, 112(6), 1198–1213.
- Sodt, A. J., Sandar, M. L., Gawrisch, K., Pastor, R. W., & Lyman, E. (2014). The molecular structure of the liquid-ordered phase of lipid bilayers. *Journal of the American Chemical Society*, 136(2), 725–732.
- Steinbach, P. J., & Brooks, B. R. (1994). New spherical-cutoff methods for long-range forces in macromolecular simulation. *Journal of Computational Chemistry*, 15(7), 667–683.
- Steinkühler, J., Sezgin, E., Urbančič, I., Eggeling, C., & Dimova, R. (2019). Mechanical properties of plasma membrane vesicles correlate with lipid order, viscosity and cell density. Communications Biology, 2(1), 337.
- The PLUMED consortium. (2019). Promoting transparency and reproducibility in enhanced molecular simulations. *Nature Methods*, 16(8), 670–673.
- Tribello, G. A., Bonomi, M., Branduardi, D., Camilloni, C., & Bussi, G. (2014). PLUMED 2: New feathers for an old bird. *Computer Physics Communications*, 185(2), 604–613.
- Usery, R. D., Enoki, T. A., Wickramasinghe, S. P., Nguyen, V. P., Ackerman, D. G., Greathouse, D. V., ... Feigenson, G. W. (2018). Membrane bending moduli of coexisting liquid phases containing transmembrane peptide. *Biophysical Journal*, 114(9), 1–13.
- Van Duyl, B. Y., Rijkers, D. T. S., Kruijff, B. De, & Killian, J. A. (2002). Influence of hydrophobic mismatch and palmitoylation on the association of transmembrane α-helical peptides with detergent-resistant membranes. FEBS Letters, 523(1–3), 79–84.
- Veatch, S. L., & Keller, S. L. (2003). Separation of liquid phases in giant vesicles of ternary mixtures of phospholipids and cholesterol. *Biophysical Journal*, 85(5), 3074–3083.
- Veatch, S. L., Soubias, O., Keller, S. L., & Gawrisch, K. (2007). Critical fluctuations in domain-forming lipid mixtures. Proceedings of the National Academy of Sciences of the United States of America, 104(45), 17650–17655.
- Venable, R. M., Ingólfsson, H. I., Lerner, M. G., Perrin, B. S., Camley, B. A., Marrink, S. J., ... Pastor, R. W. (2017). Lipid and peptide diffusion in bilayers: The Saffman-Delbrück model and periodic boundary conditions. *Journal of Physical Chemistry B*, 121(15), 3443–3457.
- Wu, E. L., Cheng, X., Jo, S., Rui, H., Song, K. C., Davila-Contreras, E. M., ... Im, W. (2014). CHARMM-GUI membrane builder toward realistic biological membrane simulations. *Journal of Computational Chemistry*, 35(27), 1997–2004.
- Wüstneck, R., Perez-Gil, J., Wüstneck, N., Cruz, A., Fainerman, V. B., & Pison, U. (2005). Interfacial properties of pulmonary surfactant layers. Advances in Colloid and Interface Science, 117(1-3), 33-58.
- Zhang, W., Trible, R. P., & Samelson, L. E. (1998). LAT palmitoylation: Its essential role in membrane microdomain targeting and tyrosine phosphorylation during T cell activation. *Immunity*, *9*(2), 239–246.
- Zhang, Z., Lu, L., & Berkowitz, M. L. (2008). Energetics of cholesterol transfer between lipid bilayers. *Journal of Physical Chemistry B*, 112(12), 3807–3811.